An absence of lamin B1 in migrating neurons causes nuclear membrane ruptures and cell death

Natalie Y. Chen[a], Ye Yang[a], Thomas A. Weston[a], Jason N. Belling[b,c], Patrick Heizer[a], Yiping Tu[a], Paul Kim[a], Lovelyn Edillo[a], Steven J. Jonas[d,e,f], Paul S. Weiss[b,c,g,h], Loren G. Fong[a,1,2], and Stephen G. Young[a,i,j,1,2]

[a]Department of Medicine, David Geffen School of Medicine, University of California, Los Angeles, CA 90095; [b]California NanoSystems Institute, David Geffen School of Medicine, University of California, Los Angeles, CA 90095; [c]Department of Chemistry and Biochemistry, David Geffen School of Medicine, University of California, Los Angeles, CA 90095; [d]Department of Pediatrics, David Geffen School of Medicine, University of California, Los Angeles, CA 90095; [e]Children's Discovery and Innovation Institute, University of California, Los Angeles, CA 90095; [f]Eli and Edythe Broad Center of Regenerative Medicine and Stem Cell Research, University of California, Los Angeles, CA 90095; [g]Department of Bioengineering, University of California, Los Angeles, CA 90095; [h]Department of Materials Science and Engineering, University of California, Los Angeles, CA 90095; [i]Department of Human Genetics, David Geffen School of Medicine, University of California, Los Angeles, CA 90095; and [j]Molecular Biology Institute, David Geffen School of Medicine, University of California, Los Angeles, CA 90095

Contributed by Stephen G. Young, November 4, 2019 (sent for review October 3, 2019; reviewed by William T. Dauer and Howard J. Worman)

Deficiencies in either lamin B1 or lamin B2 cause both defective migration of cortical neurons in the developing brain and reduced neuronal survival. The neuronal migration abnormality is explained by a weakened nuclear lamina that interferes with nucleokinesis, a nuclear translocation process required for neuronal migration. In contrast, the explanation for impaired neuronal survival is poorly understood. We hypothesized that the forces imparted on the nucleus during neuronal migration result in nuclear membrane (NM) ruptures, causing interspersion of nuclear and cytoplasmic contents—and ultimately cell death. To test this hypothesis, we bred *Lmnb1*-deficient mice that express a nuclear-localized fluorescent *Cre* reporter. Migrating neurons within the cortical plate of E18.5 *Lmnb1*-deficient embryos exhibited NM ruptures, evident by the escape of the nuclear-localized reporter into the cytoplasm and NM discontinuities by electron microscopy. The NM ruptures were accompanied by DNA damage and cell death. The NM ruptures were not observed in nonmigrating cells within the ventricular zone. NM ruptures, DNA damage, and cell death were also observed in cultured *Lmnb1*$^{-/-}$ and *Lmnb2*$^{-/-}$ neurons as they migrated away from neurospheres. To test whether mechanical forces on the cell nucleus are relevant to NM ruptures in migrating neurons, we examined cultured *Lmnb1*$^{-/-}$ neurons when exposed to external constrictive forces (migration into a field of tightly spaced silicon pillars). As the cells entered the field of pillars, there were frequent NM ruptures, accompanied by DNA damage and cell death.

nuclear lamins | nuclear envelope | nuclear membrane rupture | B-type lamins

For several decades, the prevailing view among cell biologists was that B-type lamins (lamin B1 and lamin B2) play multiple essential roles in the cell nucleus, including in DNA replication and mitosis (1–7). Over the past decade, studies of genetically modified mouse models have cast considerable doubt on this view (8–12). For example, the fact that a deficiency of both lamin B1 and lamin B2 in keratinocytes (a rapidly dividing cell type) has no perceptible effect on the skin or hair of mice is inconsistent with B-type lamins having essential roles in DNA replication or mitosis (8). Perhaps more importantly, the analysis of mouse models yielded fresh insights into the functional relevance of B-type lamins in mammals. For example, a combination of immunohistochemical studies and BrdU birthdating experiments revealed defective migration of cortical neurons in lamin B1- and lamin B2-deficient embryos, resulting in a neuronal layering abnormality in the cerebral cortex along with neonatal mortality (10–13).

Finding that B-type lamins have a role in neuronal migration was unexpected, particularly in light of prevailing views about the role of B-type lamins in cell biology (3, 5, 14–16), but in hindsight the neurodevelopmental abnormalities made sense. The migration of neurons from the ventricular zone to the cortical plate during embryogenesis depends on nucleokinesis—a process in which the cell nucleus is moved forward by cytoplasmic motors toward the leading edge of migrating neurons (17–21). In the setting of lamin B1 or lamin B2 deficiency, the nuclear envelope is weakened and nucleokinesis is impaired. Elongated nuclei or nuclei with large blebs were present in cortical neurons, both in mutant mouse embryos and mutant neurospheres (12, 22), suggesting that cytoplasmic motors were effective in pulling on the nucleus (as judged by the distorted nuclear shape) but less effective in moving the nucleus toward the leading edge of the cell

In addition to the neuronal migration defect in *Lmnb1*- and *Lmnb2*-deficient mice, there was a more perplexing phenotype—reduced neuronal density in the cerebral cortex. This loss of cortical neurons was mild in *Lmnb2*-deficient embryos but severe in *Lmnb1*-deficient embryos (11, 12). The explanation for the reduced cellularity in the cerebral cortex was not clear, but the fact that the phenotype progressed after birth in forebrain-specific *Lmnb1* and *Lmnb2* knockout (KO) mice (12) implied that it was likely a consequence of reduced neuronal survival.

We hypothesized that reduced neuronal survival in *Lmnb1* and *Lmnb2* knockout mice might be caused by reduced integrity

Significance

Deficiencies in lamin B1 or lamin B2 in mice result in markedly reduced neuronal density in the cerebral cortex, but the mechanism has been unclear. We found that deficiencies of either lamin B1 or lamin B2 cause nuclear membrane (NM) ruptures in migrating neurons, accompanied by DNA damage and cell death. Our studies were informative because they uncovered large differences in the frequency of NM repair in lamin B1- and lamin B2-deficient neurons, implying unique functions for the 2 nuclear lamins in maintaining NM integrity. Also, our studies uncovered an important role for mechanical stresses in eliciting NM ruptures, helping to explain the increased frequency of NM ruptures in migrating neurons.

Author contributions: N.Y.C., P.S.W., L.G.F., and S.G.Y. designed research; N.Y.C., Y.Y., T.A.W., J.N.B., P.H., Y.T., P.K., L.E., and S.J.J. performed research; N.Y.C. contributed new reagents/analytic tools; N.Y.C., L.G.F., and S.G.Y. analyzed data; and N.Y.C. and S.G.Y. wrote the paper.

Reviewers: W.T.D., University of Michigan; and H.J.W., Columbia University.

The authors declare no competing interest.

[1]L.G.F. and S.G.Y. contributed equally to this work.

[2]To whom correspondence may be addressed. Email: lfong@mednet.ucla.edu or sgyoung@mednet.ucla.edu.

This article contains supporting information online at https://www.pnas.org/lookup/suppl/doi:10.1073/pnas.1917225116/-/DCSupplemental.

First published December 3, 2019.

of the nuclear membranes, resulting in nuclear membrane (NM) ruptures, intermixing of nuclear and cytoplasmic contents, DNA damage, and ultimately cell death. This scenario seemed possible, for 2 reasons. First, reducing nuclear lamin expression in tumor cell lines or fibroblasts renders the cells more susceptible to NM ruptures in response to external mechanical forces (23–27), and it seemed plausible that the forces imparted on the nucleus during nucleokinesis (or the constrictive forces imparted on cells as they migrate to the cortical plate) could have similar consequences, particularly when the nuclear envelope is weakened by the absence of a B-type lamin. Second, unlike peripheral cell types, migrating neurons in the developing brain do not express lamin A or lamin C (13, 28–30), and the absence of those protein likely renders neurons more susceptible to NM ruptures.

In the current study, we took advantage of both genetically modified mice and cultured cell models to examine the hypothesis that deficiencies in B-type lamins render neurons susceptible to NM ruptures and ultimately to cell death.

Results

NM Ruptures in Neurons of *Lmnb1*-Deficient Mice. To investigate the reduced density of cortical neurons in *Lmnb1*-deficient embryos, we stained the cerebral cortex of embryonic day 18.5 (E18.5) *Lmnb1*-deficient embryos for active caspase 3, a marker of apoptotic cell death. Substantial amounts of caspase 3 staining were observed within the cortical plate of *Lmnb1*-deficient embryos (Fig. 1*A*). Also, staining with the LIVE/DEAD fluorescent vital dye revealed widespread cell death in the forebrain (but not cerebellum) of forebrain-specific *Lmnb1* knockout embryos (Fig. 1*B*). We suspected that the cell death might be a consequence of NM ruptures and intermixing of nuclear and cytoplasmic contents. To explore that idea, we bred *Lmnb1*-deficient mice harboring a nuclear-localized fluorescent reporter (*SI Appendix*, Fig. S1). In neurons of wild-type (WT) mice, the reporter was confined to the cell nucleus (Fig. 1 *C* and *D* and *SI Appendix*, Fig. S2, *Upper*). However, in *Lmnb1*-deficient embryos, we observed escape of the reporter into the cytoplasm of many neurons (Fig. 1 *C* and *E* and *SI Appendix*, Fig. S2, *Lower*). Interestingly, no NM ruptures were observed in cells of the ventricular zone (Fig. 1 *C* and *E* and *SI Appendix*, Fig. S3). By transmission electron microscopy (EM), we had no difficulty identifying discontinuities in the nuclear membranes of cortical plate neurons in *Lmnb1*-deficient embryos (Fig. 1 *F* and *G* and *SI Appendix*, Fig. S1).

NM ruptures in cortical plate neurons of *Lmnb1*-deficient embryos were accompanied by an inhomogeneous distribution of lamin B2. In cortical plate neurons, lamin B2 was mislocalized to 1 pole of the nuclear rim (*SI Appendix*, Fig. S4), leaving a large fraction of the nuclear rim devoid of nuclear lamins. In contrast, lamin B2 distribution was uniformly distributed along the nuclear rim in cells of the ventricular zone (where NM ruptures were not observed) (*SI Appendix*, Fig. S4*A*). The asymmetric distribution of lamin B2 is likely due to the forces of nucleokinesis, given that lamin B2 was largely confined to the leading edge of neurons as they migrated away from cultured neurospheres (*SI Appendix*, Fig. S4*B*) (22). In the forebrain of adult forebrain-specific *Lmnb1* knockout mice, where lamin C is expressed and lamin B2 is distributed homogeneously along the nuclear rim, NM ruptures could be detected but were infrequent (*SI Appendix*, Fig. S5).

NM Ruptures in Cultured Neurons Deficient in B-Type Lamins. To further explore the susceptibility of lamin B1- or lamin B2-deficient cells to NM ruptures, we prepared cultures of *Lmnb1*-deficient (B1KO) and *Lmnb2*-deficient (B2KO) neuronal progenitor cells (NPCs). As expected, undifferentiated and differentiated B1KO and B2KO neurons lacked lamin B1 and lamin B2, respectively (Fig. 2 *A*–*E*). Lamin C expression levels in neurons were very low relative to levels in fibroblasts (Fig. 2*A*). Prelamin A expression was even lower (Fig. 2*A*). Prelamin A mRNA expression in neurons is virtually abolished by a neuron-specific microRNA (miR-9) (28, 29). Nuclei in B1KO neurons were slightly smaller and more circular than wild-type or B2KO neurons (Fig. 2*F*).

To examine the susceptibility of cultured neurons to NM ruptures, we transduced NPCs with a nuclear-localized green fluorescent cell reporter (NLS-GFP). We then quantified NM ruptures (escape of the NLS-GFP into the cytoplasm) in wild-type, B1KO, and B2KO neurons during 50 h of live-cell imaging. NM ruptures were frequent in B1KO neurons (Movie S1), occurring in >60% of neurons examined (Fig. 3*B*). In many neurons, NM ruptures occurred repetitively, with multiple cycles of NM rupture (escape of NLS-GFP into the cytoplasm) and NM repair (return of NLS-GFP into the nucleus) (Movies S2 and S3). Thus, the total number of NM ruptures was ∼2.7-fold greater than the number of neurons examined (Fig. 3*C* and *SI Appendix*, Fig. S6). The average duration of NM ruptures was 2.9 h (Fig. 3*D*). The increased susceptibility of B1KO neurons to NM ruptures was documented in 5 independent experiments (*SI Appendix*, Fig. S6). No ruptures were detected in wild-type neurons (Fig. 3 *B* and *C*). One-third of the B1KO neurons that exhibited a NM rupture (50 of 150 neurons) died during the 50-h period of observation (*SI Appendix*, Fig. S7).

NM ruptures were also observed in B2KO neurons (Fig. 3*A*), but the pattern was distinct. First, NM ruptures were infrequent in B2KO neurons, occurring in only 7.8% of neurons during 50 h of imaging (25 NM ruptures in 321 neurons examined) (Fig. 3*B*). Second, NM repair never occurred in B2KO neurons (Fig. 3*C* and Movies S4 and S5); thus, the mean duration of NM ruptures in B2KO neurons was much longer than in B1KO neurons (38.9 h) (Fig. 3*D*). Third, NM ruptures in B2KO cells led to cell death (with fragmentation of the nucleus and detachment of the neuron from the plate) (*SI Appendix*, Fig. S7). The majority of B2KO neurons that exhibited a NM rupture died during the 50-h period of observation (17 of 25 neurons) (Fig. 3*E*). The other 8 neurons with a NM rupture remained alive, without evidence of NM repair, when the experiment was terminated after 50 h of imaging.

Cell death in cultured B1KO and B2KO neurons was evident by caspase 3 staining and staining with the LIVE/DEAD vital dye (Fig. 4 *A* and *B* and *SI Appendix*, Fig. S8). As expected, the cell death phenotype was more severe in B1KO neurons. We also observed DNA damage in B1KO and B2KO neurons, as judged by staining for γH2AX, a marker for double-stranded DNA breaks (Fig. 4*C*).

Overexpression of Lamin B2 in B1KO Neurons Does Not Eliminate NM Ruptures. Lee et al. (31) showed previously that overexpression of lamin B2 in *Lmnb1*-deficient mouse embryos did not prevent neurodevelopmental abnormalities or the perinatal death. However, the overexpression of lamin B2 significantly increased the size of *Lmnb1*-deficient mouse embryos (31), implying that the surplus lamin B2 improved the viability of *Lmnb1*-deficient cells. To test the ability of lamin B2 to compensate for the loss of lamin B1, we used a doxycycline (Dox)-inducible lentiviral vector to overexpress lamin B2 in B1KO and B2KO neurons. In the presence of doxycycline, lamin B2 expression in B1KO neurons was robust (Fig. 5*A*), such that the lamin B2 covered the entire nuclear rim rather than only 1 pole of the nucleus (Fig. 5*B*). Overexpression of lamin B2 reduced the frequency of NM ruptures in B1KO cells, but many of the neurons continued to have NM ruptures (Fig. 5 *C* and *D*). Indeed, some B1KO neurons had repetitive NM ruptures (Fig. 5 *C* and *D*). In contrast, overexpression of lamin B2 in B2KO cells eliminated NM ruptures (Fig. 5 *C* and *D*). Lamin B2 overexpression also abolished cell death in B2KO cells (reduced the frequency of cell death to that observed in wild-type neurons) (Fig. 5 *E* and *F* and *SI Appendix*, Fig. S9). Overexpression of lamin B2 in B1KO neurons

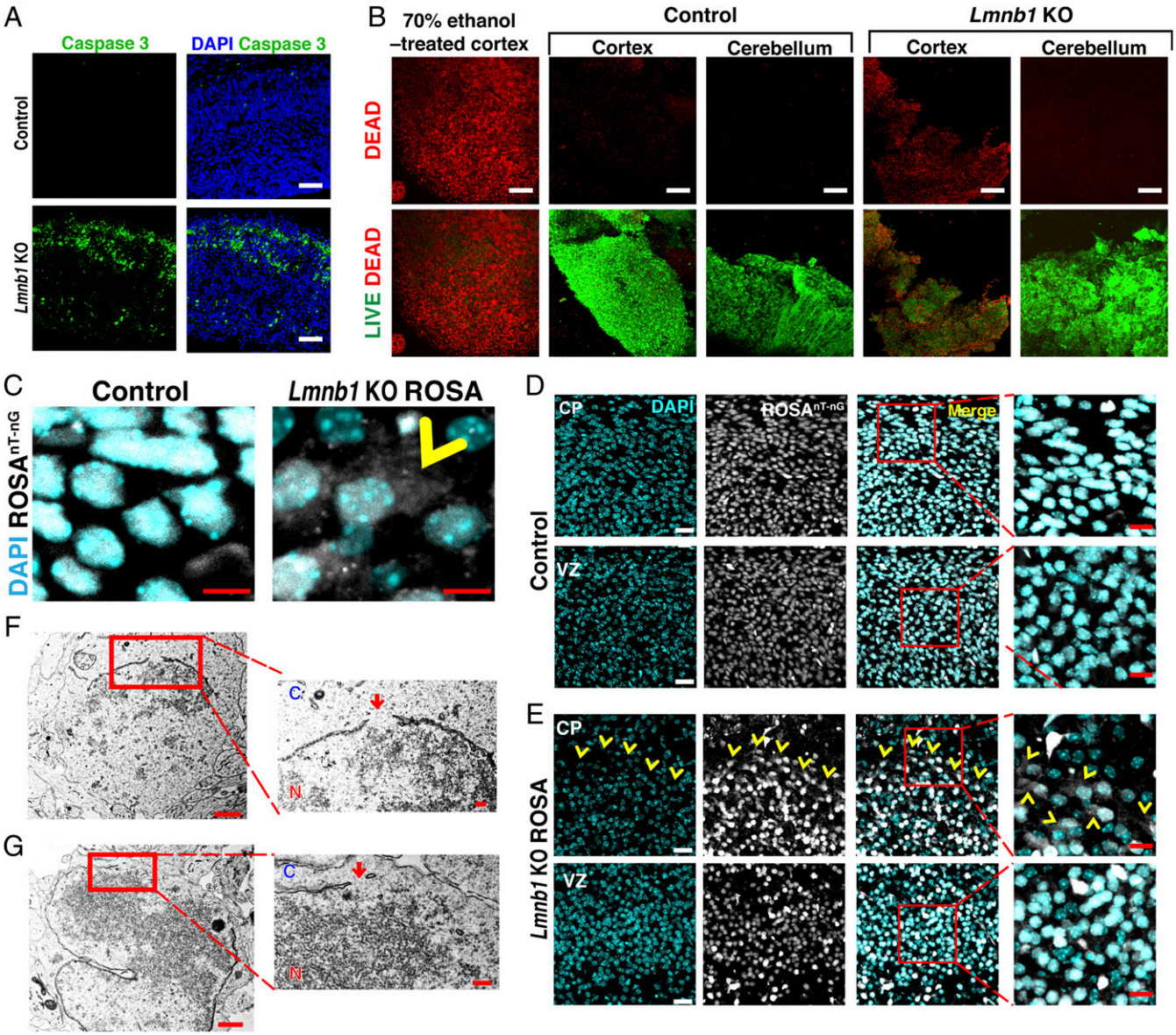

Fig. 1. Forebrain-specific inactivation of *Lmnb1* causes neuronal cell death in the cerebral cortex of mouse embryos and leads to NM ruptures. (*A*) Immunofluorescence microscopy of the cerebral cortex of E18.5 control (*Lmnb1*$^{+/+}$) and *Lmnb1* KO (*Emx1-Cre Lmnb1*$^{fl/fl}$) embryos after staining for a marker of programmed cell death (caspase 3, green). DNA was stained with DAPI (blue). (Scale bars, 50 μm.) (*B*) Immunofluorescence microscopy of the cerebral cortex and cerebellum of control (*Lmnb1*$^{+/+}$ *Lmnb2*$^{fl/fl}$) and *Lmnb1* KO (*Emx1-Cre Lmnb1*$^{fl/fl}$) E18.5 embryos after staining tissues with the LIVE/DEAD fluorescent vital dye. The LIVE/DEAD dye yields a green signal in live cells and a red signal in dead cells. As a positive control for dead cells, a wild-type mouse embryo brain was treated with 70% ethanol. (Scale bars, 100 μm.) (*C–E*) Fluorescence microscopy images of cortical neurons in control (*Lmnb1*$^{+/+}$ ROSA$^{nT\text{-}nG}$) and *Lmnb1* KO ROSA (*Emx1-Cre Lmnb1*$^{fl/fl}$ ROSA$^{nT\text{-}nG}$) E18.5 embryos. The ROSA$^{nT\text{-}nG}$ transgene produces a nuclear-targeted tdTomato reporter in the absence of *Cre* and a nuclear-targeted GFP in the presence of *Cre*. In these images, both tdTomato and GFP are colored white and the DNA (stained with DAPI) is colored cyan. *C* shows high-magnification images of cortical plate neurons in a control embryo and a *Lmnb1* KO ROSA embryo; the yellow arrowhead points to a neuron with a NM rupture (escape of the ROSA$^{nT\text{-}nG}$ reporter into the cytoplasm). (Scale bars, 5 μm.) (*D* and *E*) Images of the cortical plate (CP) and ventricular zone (VZ) of forebrains from a control embryo (*D*) and a *Lmnb1* KO ROSA embryo (*E*). In the control embryo, the ROSA$^{nT\text{-}nG}$ reporter is confined to the nucleus in CP and VZ neurons. Many CP neurons in the *Lmnb1* KO ROSA embryo had NM ruptures, with escape of the reporter protein into the cytoplasm (yellow arrowheads), but the reporter remained confined to the nucleus in VZ neurons. (Scale bars, 50 μm, except in the *Insets* where the scale bar is 10 μm.) (*F* and *G*) Electron micrographs showing NM discontinuities in cortical plate neurons of E18.5 *Lmnb1* KO (*Emx1-Cre Lmnb1*$^{fl/fl}$) embryos (red arrows). (Scale bar for low magnification images on the *Left*, 1 μm; scale bar for images on the *Right*, 200 nm.) N, nuclei; C, cytoplasm.

reduced but did not eliminate cell death (Fig. 5 *E* and *F* and *SI Appendix*, Fig. S9).

NM Ruptures and Cell Death in B1KO Cells as They Migrate into and across Tight Constrictions. We suspected that the NM ruptures and cell death in the cortical neurons of *Lmnb1*-deficient embryos resulted from mechanical forces on the cell nucleus—both internal forces associated with nucleokinesis and the constrictive forces as cells migrated between other cells within the cortical plate (32). To explore this idea, we plated wild-type and B1KO neurons onto the flat portion of a silicon wafer and observed the cells as they migrated into an adjacent field of tightly spaced pillars (exposing both the cells and cell nuclei to external constrictive forces) (Fig. 6*A* and *SI Appendix*, Fig. S10*A*). As B1KO neurons entered the

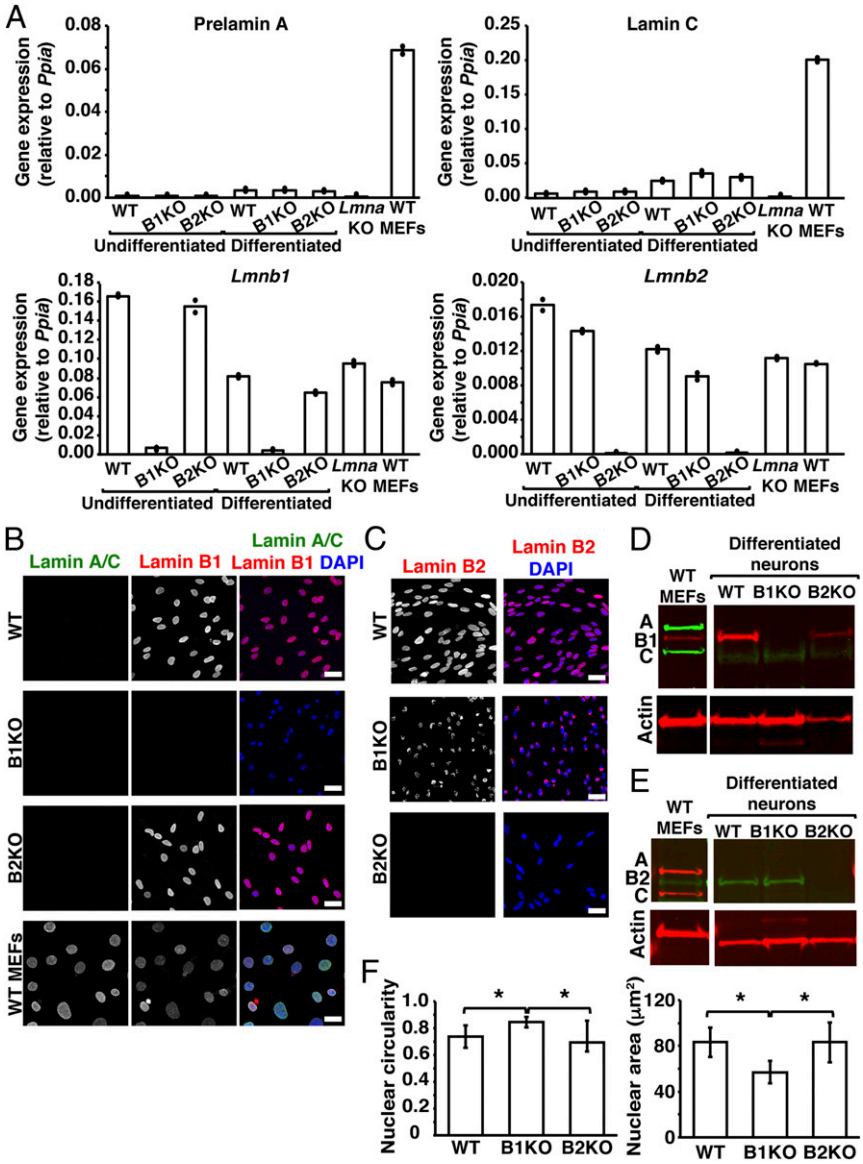

Fig. 2. Nuclear lamin expression in neuronal progenitor cells lacking lamin B1 or lamin B2. (*A*) Transcript levels for prelamin A, lamin C, lamin B1, and lamin B2 in *Lmnb1*$^{+/+}$*Lmnb2*$^{+/+}$ (WT), *Lmnb1*$^{-/-}$*Lmnb2*$^{+/+}$ (B1KO), and *Lmnb1*$^{+/+}$*Lmnb2*$^{-/-}$ (B2KO) undifferentiated and differentiated neurons. Controls included *Lmna*$^{+/+}$*Lmnb1*$^{+/+}$*Lmnb2*$^{+/+}$ mouse embryonic fibroblasts (WT MEFs) and *Lmna*$^{-/-}$ MEFs (*Lmna* KO). Expression levels were normalized to *Ppia*; bar graphs show means for 2 independent experiments and dots represent values from individual experiments. (*B* and *C*) Immunofluorescence microscopy of neurons after staining with antibodies against lamin A/C and lamin B1 (*B*) or an antibody against lamin B2 (*C*). DNA was stained with DAPI (blue). (Scale bars, 25 μm.) (*D* and *E*) Western blots of neuronal protein extracts with antibodies against lamin A/C (green) and lamin B1 (red) (*D*) or with antibodies against lamin A/C (red) and lamin B2 (green) (*E*). Actin was used as a loading control. (*F*) Bar graphs depicting nuclear circularity and nuclear area in WT, B1KO, and B2KO neurons. More than 200 cells from 3 neurospheres of each genotype were analyzed. Mean ± SD; **P* < 0.05 by an unpaired Student's *t* test.

field of pillars, we observed NM ruptures (Fig. 6*B*). No NM ruptures were observed when wild-type neurons entered the field of pillars. Also, we observed widespread caspase 3 staining of B1KO neurons after they had migrated into the field of pillars (Fig. 6*C* and *SI Appendix*, Fig. S10*B*). Cell death was also observed with the LIVE/DEAD vital dye (Fig. 6*D*).

Discussion

In earlier studies, we documented defective migration of cortical neurons in *Lmnb1* and *Lmnb2* knockout embryos, along with a second abnormality—reduced density of neurons within the cerebral cortex (12). The mechanism for the neuronal migration defect was reasonably well understood, but a mechanism for the reduced cellularity of neurons was not. In the current study, we observed frequent NM ruptures in migrating neurons in the cortical plate of E18.5 *Lmnb1*-deficient embryos, evident by the escape of a nuclear-localized fluorescent reporter protein into the cytoplasm and by electron micrographs revealing discontinuities in the nuclear membranes, but did not observe NM ruptures in the more stationary cells of the ventricular zone. The regions of the brain with NM ruptures also had many dead and dying neurons, as judged by staining for caspase 3 or by staining with the LIVE/DEAD fluorescent vital dye. Consistent with the findings in *Lmnb1*-deficient embryos, we observed NM ruptures, accompanied by DNA damage and cell death, in B1KO neurons as they migrated away from cultured neurospheres. Thus, both mouse embryo and cultured neuron observations strongly imply

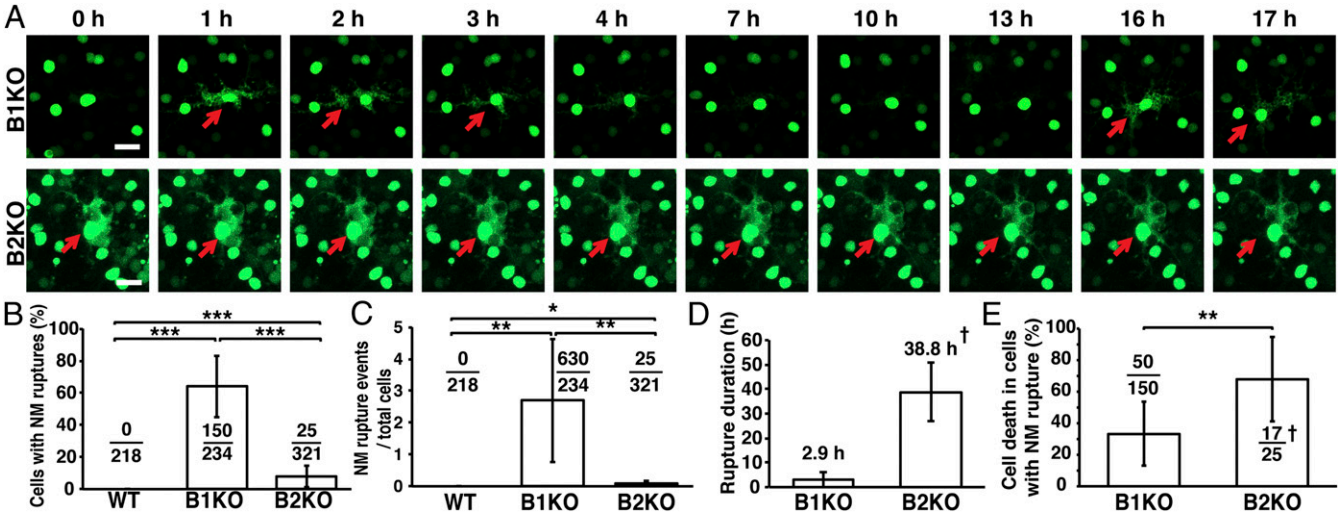

Fig. 3. NM ruptures in B1KO and B2KO neurons. (*A*) Live-cell fluorescence microscopy images of B1KO and B2KO neurons expressing a NLS-GFP. Red arrows point to a NM rupture (escape of the nuclear-localized GFP into the cytoplasm). (Scale bars, 20 μm.) (*B*) Percentages of neurons with NM ruptures in 5 independent experiments during 50 consecutive hours of imaging. The ratio depicts numbers of NM ruptures relative to total numbers of cells observed. ***$P <$ 0.0001. (*C*) Numbers of NM rupture events in 5 independent experiments, each with 50 h of imaging. Mean ± SD; *$P < 0.01$. **$P < 0.001$. One of the 5 experiments was an outlier, with 2 to 3 times more NM ruptures than in the other 4 experiments. When the outlier experiment was excluded (*SI Appendix*, Fig. S6), the SD was smaller and the levels of statistical confidence were greater. (*D*) Average duration of NM ruptures. †Repair of a NM rupture was never observed in a B2KO neuron; thus, the duration of 38.8 h represents the average length of time that NM ruptures were observed over the 50-h period of imaging. (*E*) Percentages of cells with NM ruptures that died during 50 h of imaging. The ratio depicts numbers of cells with NM ruptures that died relative to total numbers of cells with NM ruptures. †Cell death was observed in 17 of 25 B2KO neurons with a NM rupture; 8 of the 25 cells with a NM rupture remained alive, without evidence of NM repair, at the end of the 50-h period of imaging. *B–E* show mean ± SD **$P < 0.001$.

that the reduced density of cortical neurons in *Lmnb1*-deficient mice is due to NM ruptures and the accompanying cell death.

The susceptibility of *Lmnb1*-deficient neurons to NM ruptures is likely due to several factors. First, neither the cortical neurons in E18.5 embryos nor cultured neurons express *Lmna*, the gene for lamin A and lamin C. The minimal amounts of lamin A and lamin C expression in cortical neurons probably increase the likelihood of NM ruptures. On the other hand, the high levels of lamins A and C expression in skin and liver likely explains why keratinocyte- or hepatocyte-specific *Lmnb1*/*Lmnb2* knockout mice are free of pathology (8, 9). Second, while lamin B2 is expressed in neurons, it has little ability to compensate for the loss of lamin B1 (30, 31). In migrating neurons of *Lmnb1*-deficient embryos, lamin B2 is asymmetrically distributed along 1 pole of the nucleus, leaving most of the nuclear rim devoid of any nuclear lamin (*SI Appendix*, Fig. S4*B*).

NM ruptures and cell death were never observed in cells of the ventricular zone but were frequent in neurons within the cortical plate. We suspect that the higher susceptibility of cortical plate neurons to NM ruptures relates to deformational forces on the cell nucleus during neuronal migration. Neuronal migration is a saltatory process that depends on nucleokinesis—the motor-driven translocation of the nucleus into the leading edge of the cell. Following translocation of the nucleus, the trailing edge of the neuron is remodeled, resulting in net forward movement of the cell in the direction of the cortical plate. The mechanical forces involved in pulling the cell nucleus forward, together with the virtual absence of nuclear lamins over a large portion of the nucleus, likely triggers NM ruptures. Two observations favor a role for mechanical forces in eliciting NM ruptures. First, NM ruptures were not observed in more stationary cells of the ventricular zone, where the long-distance migration of neurons along glial-directed guides is not in play. Second, NM ruptures, along with cell death, were elicited when cultured B1KO neurons migrated into a field of tightly spaced silicon pillars. The nuclear membrane ruptures in the "silicon pillar experiments" could be a result of nucleokinesis forces and/or a direct consequence of the compressive forces that accompany cellular migration through the field of narrowly spaced pillars.

Lamin B1 and lamin B2 are ∼60% identical at the amino acid level (33), and their temporal and spatial patterns of expression in the brain are very similar (12). Those considerations, along with the fact that deficiencies in either protein cause neuronal layering abnormalities in the cerebral cortex, might lead one to suspect that the 2 nuclear lamins have identical functions. Any such view, however, would be inconsistent with other observations. First, the properties of the 2 proteins are different. For example, lamin B1 is essential for a uniform distribution of lamin B2 along the nuclear rim, whereas the distribution of lamin B1 is quite normal in the absence of lamin B2 (12). Second, lamin B1's farnesyl lipid anchor is required for development of the brain and for survival, whereas lamin B2's farnesyl lipid anchor appears to be utterly dispensable (22). *Lmnb1* knockin embryos that express a nonfarnesylated lamin B1 manifest severe neuronal layering abnormalities in the cerebral cortex as well as perinatal death—like conventional *Lmnb1* knockout mice (22). In contrast, *Lmnb2* knockin mice that express a nonfarnesylated lamin B2 are entirely healthy, free of both neurodevelopmental abnormalities and perinatal mortality (22). Third, the characterization of "reciprocal *Lmnb1*/*Lmnb2* knockin mice" revealed that lamin B1 and lamin B2, despite high levels of amino acid identity, have minimal capacities to substitute for each other during development. For example, $Lmnb2^{+/+}Lmnb1^{B2/B2}$ embryos, where the gene-regulatory elements of *Lmnb1* drive the expression of lamin B2 (resulting in substantially increased levels of lamin B2 expression but no lamin B1), manifest severe neuronal migration defects, reduced neuronal density in the cerebral cortex, and perinatal death. However, brain weights in $Lmnb2^{+/+}Lmnb1^{B2/B2}$ embryos were ∼60% higher than in conventional *Lmnb1* knockout embryos (31), implying that greater-than normal amounts of lamin B2 expression have at least some capacity to improve the survival of *Lmnb1*-deficient neurons.

Our cultured neuron studies underscored the limited capacity of lamin B2 to substitute for lamin B1. Overexpression of lamin

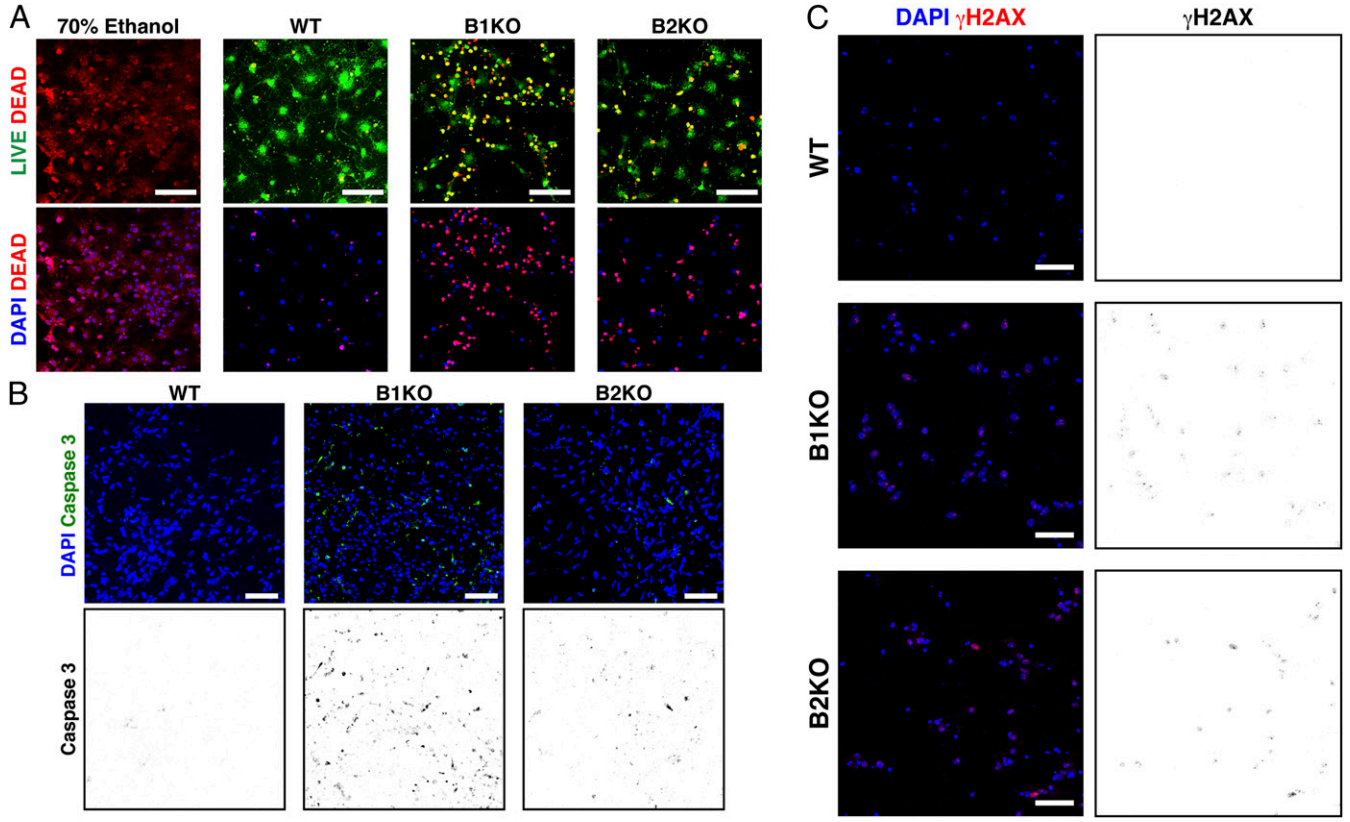

Fig. 4. Cell death in cultured B1KO and B2KO neurons. (*A*) Fluorescence microscopy of WT (*Lmnb1*$^{+/+}$ *Lmnb2*$^{fl/fl}$), B1KO, and B2KO neurons after staining with the LIVE/DEAD vital dye. The LIVE/DEAD dye fluoresces green in live cells and red in dead cells. As a control for dead cells, we treated wild-type neurons with 70% ethanol. DNA was stained with DAPI (blue). (Scale bars, 20 μm.) (*B*) Immunofluorescence microscopy of WT, B1KO, and B2KO neurons that had been cultured in Matrigel for 7 d and stained with an antibody marker of programmed cell death (caspase 3, green). DNA was stained with DAPI (blue). (Scale bars, 25 μm.) The *Lower* shows caspase 3 staining in black against a white background. (*C*) Immunofluorescence microscopy of WT, B1KO, and B2KO differentiated neurons that had been cultured for 30 d and then stained with an antibody against the DNA damage marker γH2AX (red). DNA was stained with DAPI (blue). (Scale bars, 50 μm.) The panels on the *Right* show caspase 3 staining in black against a white background.

B2 in B1KO neurons reduced but did not prevent NM ruptures and cell death, despite the fact that the lamin B2 covered the entire nuclear rim. In contrast, lamin B2 overexpression in B2KO neurons abolished NM ruptures.

Our analysis of NM ruptures in B1KO and B2KO neurons by live-cell microscopy suggested distinct functions for lamin B1 and lamin B2. NM ruptures occurred in most B1KO neurons and repetitively in a subset of neurons, with repeated cycles of NM rupture and repair (escape of the fluorescent reporter into the cytoplasm followed by return of the reporter into the nucleus). The mean duration of NM ruptures in B1KO neurons was 2.9 h. Some B1KO neurons with NM ruptures died, but the majority survived. The behavior of B2KO neurons was different. NM ruptures were much less frequent but when they occurred they were never repaired and resulted in cell death. We do not understand the phenotypic differences, but our studies suggest that lamin B1 is more important for the structural integrity of the nuclear envelope, whereas lamin B2 is crucial for NM repair. Perhaps lamin B2 is the "mortar" that binds together the key building blocks in the nuclear lamina (i.e., lamin B1), and perhaps lamin B2 (or a lamin B2-interacting protein) plays a key role in sealing holes in the nuclear membranes.

The phenotype observed in B2KO neurons—infrequent NM ruptures but an absence of NM repair—may help to explain phenotypes observed in *Lmnb2* mouse models. In conventional *Lmnb2* knockout embryos, the reduction in the size of the cerebral cortex is modest (only ~5 to 10% smaller than in wild-type embryos) (11). In contrast, the reduction in the size of the forebrain in 4-mo-old forebrain-specific *Lmnb2* knockout mice is more substantial (20% smaller than in wild-type mice) (12). The subtle decrease in cortical size in E18.5 *Lmnb2* knockout embryos may reflect infrequent NM ruptures (and the resulting cell death), whereas the more substantial decrease in cortical size in the adult forebrain-specific *Lmnb2* knockout mice could reflect loss of neurons due to an absence of NM repair. Even if NM ruptures are infrequent, the failure to repair the ruptures would be expected to result in a progressive loss of neurons and brain size.

Finally, we would point out that the 2 principal phenotypes associated with deficiencies of B-type lamins, neuronal layering defects in the cortex and decreased neuronal survival, are mechanistically related. Fundamental to both are a weakened nuclear lamina and mechanical forces on migrating neurons during development. Interestingly, B-type lamin deficiencies have only minor effects on stationary, postmitotic, *Lmna*-expressing neurons (13, 28). Inactivating *Lmnb1* in photoreceptor neurons of the retina early in development leads to neuronal layering abnormalities and a dramatic loss of neurons, whereas inactivating both *Lmnb1* and *Lmnb2* in postmitotic photoreceptor cells after birth has minimal consequences (minor effects on the positioning of the nucleus within the cell) (34, 35). The B-type lamins are long-lived proteins with a half-life of over 5 mo in postmitotic cells (36), making it challenging to define the functional relevance of the proteins in adult mice (37).

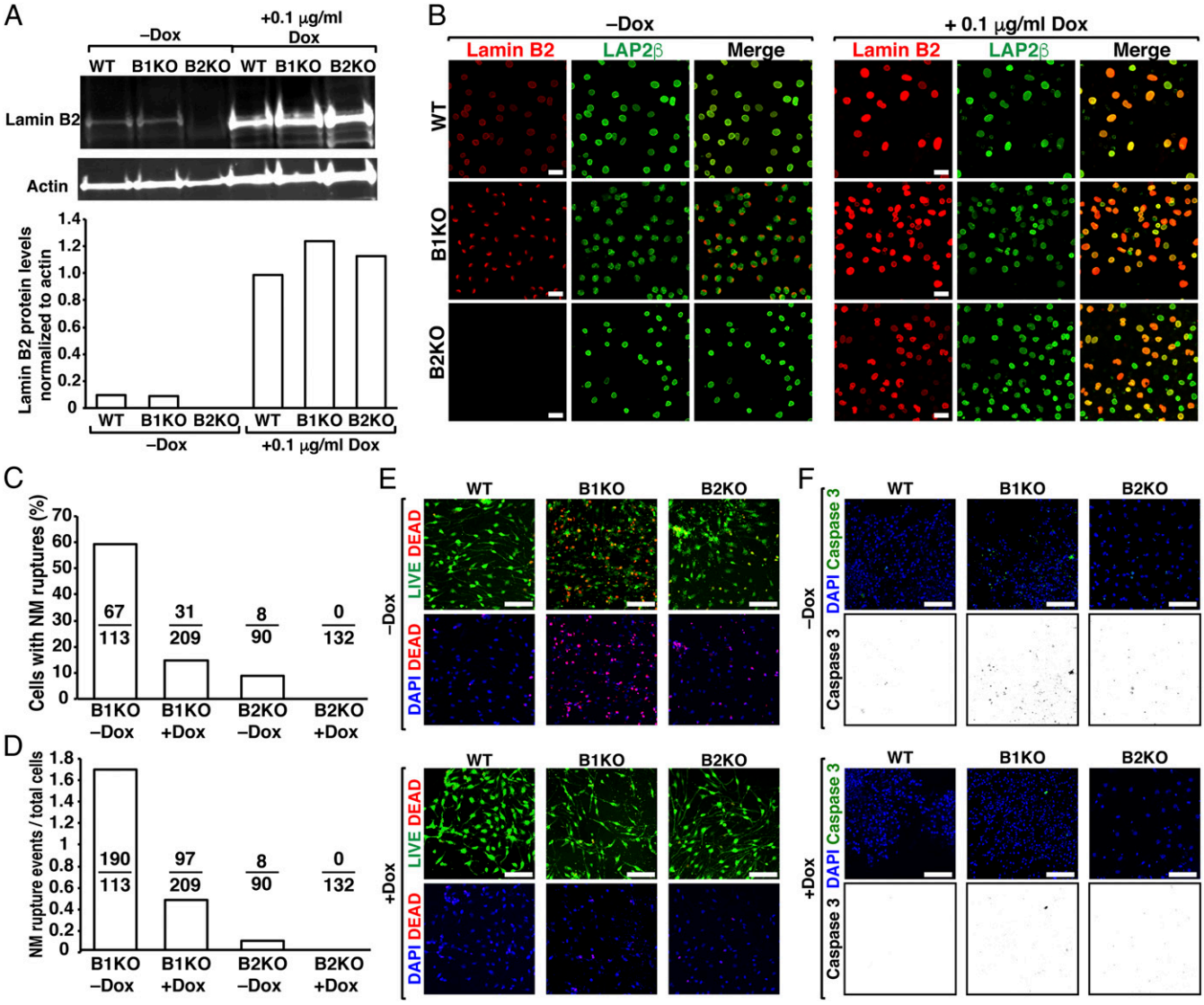

Fig. 5. Overexpression of lamin B2 reduces cell death and NM ruptures in B1KO and B2KO neurons. (*A*) Western blots of extracts from WT, B1KO, and B2KO neurons; the neurons had been transduced with a doxycycline-inducible lamin B2 lentiviral vector (pTRIPZ-*LMNB2*) and then incubated in the presence or absence of Dox. Actin was used as a loading control. The bar graph shows lamin B2 protein levels normalized to actin. (*B*) Immunofluorescence microscopy of WT, B1KO, and B2KO neurons that had been transduced with pTRIPZ-*LMNB2*. In the presence of Dox, the cells expressed lamin B2. Immunofluorescence microscopy was performed after staining neurons with antibodies against lamin B2 (red) and LAP2β (green). (Scale bars, 20 μm.) (*C*) Percentages of B1KO and B2KO neurons exhibiting NM ruptures during 20 h of live-cell imaging. Ratios show numbers of neurons with NM ruptures over the total number of neurons examined. (*D*) Total numbers of NM rupture events relative to the total number of neurons examined. In these studies, the neurons had been transduced with NLS-GFP and pTRIPZ-*LMNB2* and incubated in the presence or absence of Dox. NM ruptures (escape of NLS-GFP in the cytoplasm) were observed by fluorescence microscopy. Data show totals from 2 independent experiments. (*E*) Overexpression of lamin B2 in B1KO and B2KO neurons reduces cell death, as judged by staining with the LIVE/DEAD fluorescent vital dye. WT, B1KO, and B2KO neurons that had been transduced with pTRIPZ-*LMNB2* were incubated in the presence or absence of Dox for 24 h and then incubated with the LIVE/DEAD dye, which fluoresces green in live cells and red in dead cells. DNA was stained with DAPI (blue). (Scale bars, 50 μm.) (*F*) Overexpression of lamin B2 in B1KO and B2KO neurons reduces programmed cell death, as judged by staining for caspase 3. WT, B1KO, and B2KO neurons that had been transduced with pTRIPZ-*LMNB2* were incubated in the presence or absence of Dox for 24 h and then stained with a caspase 3-specific antibody (green). No caspase 3 staining was observed in WT cells. DNA was stained with DAPI (blue). (Scale bars, 50 μm.) The *Lower* shows caspase 3 staining in black against a white background.

Materials and Methods

Cell Culture Models. NPCs were isolated from E13.5 embryos derived from intercrossing *Lmnb1*$^{+/-}$ mice and used to generate *Lmnb1*$^{+/+}$*Lmnb2*$^{+/+}$ (WT) and *Lmnb1*$^{-/-}$*Lmnb2*$^{+/+}$ (B1KO) neurospheres. Explants from the cerebral cortex were placed in DMEM/F-12 medium (Corning) and dissociated with TrypLE Select (Gibco); the NPCs were resuspended in DMEM/F-12 (Corning). To generate *Lmnb1*$^{+/+}$*Lmnb2*$^{-/-}$ (B2KO) neurospheres, we intercrossed *Emx1-Cre Lmnb2*$^{fl/fl}$ mice and isolated forebrain NPCs from *Emx1-Cre Lmnb2*$^{fl/fl}$ embryos. To be certain that *Lmnb2* was completely inactivated, the NPCs were treated twice with *Cre* adenovirus (1,000 multiplicity of infection). Neurospheres were generated by culturing NPCs in DMEM/F-12 medium containing 2% B-27 supplement (Thermo Fisher Scientific), 100 U/mL of penicillin, and 100 μg/mL of streptomycin at 37 °C in 5 to 7% CO_2. Neurospheres were supplemented with 3 μL of a heparin–embryonic growth factor (EGF)–fibroblast growth factor (FGF) mix (described below) for every milliliter of medium. NPCs were transduced (in University of California, Los Angeles [UCLA]'s Vector Core Facility) with a lentiviral vector for NLS-GFP (26).

Preparing the Heparin–EGF–FGF Supplement. One milligram of FGF was resuspended in 1 mL of FGF buffer (0.1% BSA [Sigma] in PBS) and diluted in 39 mL of DMEM/F-12 (Corning); 1 mg EGF (Thermo Fisher Scientific) was

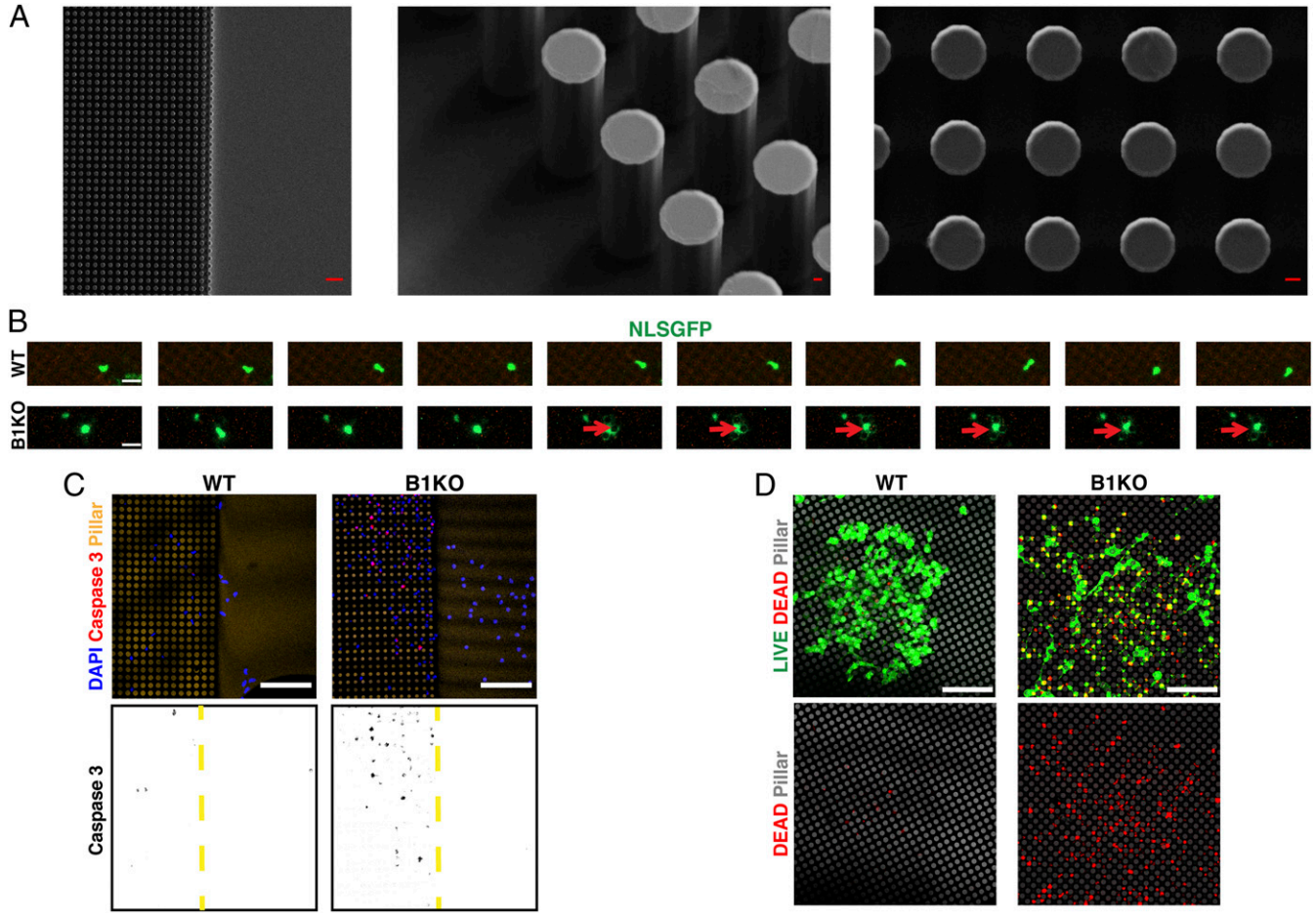

Fig. 6. NM ruptures and cell death during the migration of B1KO neurons into a field of silicon pillars (8 μm in diameter; 22 μm in height; spaced 4 μm apart). (*A*, *Left*) Scanning electron micrograph of a silicon wafer (with one side flat and the other side patterned with uniformly spaced silicon pillars). (Scale bar, 30 μm.) (*A*, *Middle* and *Right*) Scanning electron micrographs of the uniformly spaced silicon pillars. (Scale bars, 2 μm.) (*B*) Live-cell fluorescence microscopy images (20-min intervals) of NLS-GFP–expressing WT and B1KO neurons after the cells had migrated into the field of pillars. NM ruptures (escape of the NLS-GFP into the cytoplasm) were observed in B1KO neurons (red arrows; *Bottom*) but not in WT neurons (*Top*). (Scale bars, 20 μm.) (*C*) Immunofluorescence microscopy of WT and B1KO neurons with a caspase 3-specific antibody (a marker of apoptotic cell death). Neurospheres were pipetted onto the smooth portion of the silicon wafer, and individual neurons were allowed to migrate into the field of pillars. The migration of neurons into the field of pillars subjects the cells as well as the cell nucleus to constrictive forces. Cell death, as judged by caspase 3 staining, was observed in B1KO neurons (but not WT neurons) after the cells had migrated into the field of pillars. DNA was stained with DAPI (blue). (Scale bars, 50 μm.) The panels below show caspase 3 staining in black against a white background. The edge of the field of pillars is marked by a yellow dashed line. (*D*) Fluorescence microscopy with the LIVE/DEAD fluorescent vital dye, revealing cell death in B1KO neurons (but not WT neurons) after the migration of cells into the field of pillars. The LIVE/DEAD fluorescent vital dye fluoresces green in live cells and red in dead cells. (Scale bar, 50 μm.)

resuspended in EGF buffer (10% BSA in PBS) and diluted in 9 mL of fresh DMEM/F-12; 500 mg of heparin sodium salt (Sigma-Aldrich) was dissolved in 100 mL DMEM/F-12. To prepare 25 mL of the heparin–EGF–FGF supplement, 8 mL of the FGF solution, 5 mL of the EGF solution, and 10 mL of the heparin solution were mixed with 2 mL of DMEM/F-12.

Neuronal Differentiation. Cultured neurospheres were carefully removed with polyethylene pipets (Fisher) and pipetted into a single drop of laminin (Sigma-Aldrich) on poly-L-ornithine–coated plates Neurospheres were allowed to settle for 30 min at 37 °C and then incubated with the DMEM/F-12 containing 2% B-27 supplement, 100 U/mL of penicillin, and 100 μg/mL of streptomycin. Neurospheres were differentiated for up to 30 d.

Quantitative RT-PCR Studies. RNA was isolated from undifferentiated and differentiated neurospheres, treated with DNase I (Ambion), and reverse transcribed with random primers, oligo(dT), and SuperScript III (Invitrogen). qPCR reactions were performed on a 7900 Fast Real-Time PCR system (Applied Biosystems) with SYBR Green PCR Master Mix (Bioline). Transcript levels were determined by the comparative cycle threshold method and normalized to levels of cyclophilin A. All primers used are listed in the *SI Appendix*, Table S1.

Immunocytochemistry. Neurons that had been differentiated on coverslips were fixed with 4% paraformaldehyde in PBS or ice-cold methanol, dipped once in acetone, and permeabilized with 0.2% Triton. The fixed cells were then processed for confocal immunofluorescence microscopy (8) with the antibodies listed in *SI Appendix*, Table S2. For confocal immunofluorescence microscopy, images were recorded with a Zeiss LSM 700 laser-scanning microscope with a Plan Apochromat 20×/0.80 objective (air) or a Plan Apochromat 100×/1.40 oil-immersion objective. Images along the *z* axis were processed with Zen 2010 software (Zeiss).

Western Blots. Urea-soluble protein extracts from cells were size fractionated on 4 to 12% gradient polyacrylamide Bis-Tris gels (Invitrogen) and then transferred to a nitrocellulose membrane for Western blots. Membranes were blocked with Odyssey Blocking solution (LI-COR Biosciences) for 1 h at room temperature (RT) and then incubated with primary antibodies at 4 °C overnight (antibodies are listed in *SI Appendix*, Table S2). After washing the membranes with PBS containing 0.1% Tween-20, the membranes were incubated with infrared dye (IR)-labeled secondary antibodies (LI-COR Biosciences) for 1 h at RT. The IR signals were quantified with an Odyssey infrared scanner (LI-COR Biosciences).

Nuclear Shape Analyses. To assess the area and circularity of cell nuclei, WT, B1KO, and B2KO neurospheres were stained with an antibody against the inner nuclear membrane protein LAP2β, and images of cells were recorded with a Zeiss LSM700 laser-scanning microscope (20× objective), focusing on individual neurons that had migrated away from the main body of the neurosphere. Nuclear area was assessed using ImageJ software; nuclear circularity ($4\pi \times$ area/perimeter^2) was assessed by measuring nuclear areas and perimeters for 100 cells/genotype ($n = 3$ independent experiments). Nuclear circularity reaches a maximum value of 1.0 for a perfect circle (38).

Live-Cell Imaging. Neurospheres were plated on a poly-L-ornithine–coated 6-well plate containing 2-mm glass wells (MatTek), and live-cell imaging was performed with a Zeiss LSM 800 confocal microscope equipped with a Plan Apochromat 10×/0.45 or a Plan Apochromat 20×/0.80 objective at 37 °C with 5% CO_2 (maintained with TempModule S1 CO_2 Module S1 from Zeiss). *Z* stacks were acquired from both fluorescence and transmission channels. Image sequences were analyzed with ZEN (Zeiss) using linear adjustments applied uniformly to the entire image. For confocal image stacks, images were 3-dimensionally reconstructed and displayed as maximum intensity projections. A nuclear rupture event was defined as NLS-GFP entry into the cytoplasm in interphase cells.

Fluorescent Vital Dye. Neurons were allowed to differentiate on poly-L-ornithine–coated 6-well plates containing 2-mm glass wells (MatTek) for 7 d. After washing cells with PBS (Gibco), cell viability was assessed with the LIVE/DEAD Cell Imaging Kit (Thermo Fisher). Neurons were incubated with the LIVE/DEAD dye for 15 min at 20 to 25 °C and then fixed with 4% paraformaldehyde in PBS and stained with DAPI. Cells were imaged immediately with a Zeiss LSM700 laser-scanning microscope with a Plan Apochromat 20×/0.80 objective (air). As a positive control for cell death, cells or tissue sections were treated with 70% ethanol for 15 min before staining.

Plating of Neurospheres on Matrigel. A vial of Matrigel (Corning) was thawed overnight by submerging it in ice in a 4 °C refrigerator. Using prechilled pipet tips, Matrigel was pipetted into glass-bottom 6-well culture plates (MatTek) and then incubated at 37 °C for 30 min to allow a gel to form. Neurospheres were resuspended in Matrigel and plated on top of the gel layer, allowing 30 min at 37 °C for the gel to solidify. Each well was then flooded with DMEM/F-12 medium containing 2% B-27 supplement (Thermo Fisher), 100 U/mL of penicillin, and 100 μg/mL of streptomycin. Neurons were allowed to differentiate and migrate into the Matrigel for 7 d. The neurospheres were then prepared for immunocytochemistry as described earlier.

Silicon Pillar Fabrication. Prime quality 4-inch Si (100) wafers (P/B, 1 to 10 Ω-cm) were purchased from UniversityWafer (Boston, MA). A quartz photomask (PhotomaskPortal) was designed with LayoutEditor software to fabricate a custom array of circles with 4-μm spacings and used for conventional photolithography. Positive photoresist SPR700-1.2 was spin-coated on the Si surface, followed by a 90-s soft bake at 90 °C on a hotplate. A Karl Suss contact aligner was used to expose the photoresist on the wafer selectively with the pattern on the photomask with an optimal exposure time of 2 s (UV wavelength 365 nm, intensity 12 mW/cm^2). The exposed wafer was post-exposure baked at 110 °C for 90 s, immersed in MF-26A developer for 1 min (development), rinsed with deionized water, and blown dry with N_2. After photolithography, the patterned silicon wafer was reactive-ion etched (Plasma-Thermo FDRIE DSE II) for 6 min and 30 s to remove silicon in the exposed regions, forming 22-μm-deep silicon pillars. The pillar depth, diameter, and pitch were characterized with a Zeiss Supra 40VP scanning electron microscope (SEM) and Dektak 6 Surface Profilometer.

Fluorescent Labeling of APTES-Functionalized Pillar Substrates. The silicon micropillar substrates were functionalized with (3-aminopropyl) triethoxysilane (APTES, Sigma-Aldrich) using chemical vapor deposition. Silanol groups were formed on the silicon surface by ozone treatment for 15 min. The substrate and a Teflon cap filled with 100 μL of APTES was then placed in a vacuum flask and suspended in a 40 °C water bath with a vacuum line attached. House vacuum was engaged for 1 min, reducing the pressure in the flask to vaporize APTES, promoting covalent binding between the APTES silane termination and surface silanol functionalities during a 1-h incubation. Substrates were removed from the flask and rinsed with 100% ethanol. The silicon was then labeled with a fluorescent dye (Texas Red). To generate a stock solution, 1 mg of Texas Red sufonyl chloride was mixed with 100 μL of 99% *N*,*N*-dimethylformamide (Sigma-Aldrich). A total of 50 μL of the stock was added dropwise to 10 mL of a 0.1- to 0.2-M sodium bicarbonate (Sigma-Aldrich) buffer (pH ∼ 9). The APTES-functionalized substrate was then incubated in the buffered dye solution for 2 h at 4 °C on a shaking stage. The silicon substrates were then rinsed with Milli-Q ultrapure 18 MΩ water to remove physiosorbed dye and stored at −20 °C until use. To plate neurospheres for differentiation, laminin (Sigma-Aldrich) was first pipetted onto the silicon wafer substrates; the neurospheres were removed with a polyethylene pipets (Fisher) and pipetted into a drop of laminin. Neurospheres were allowed to settle for 30 min at 37 °C and then incubated with DMEM/F-12 medium containing 2% B-27 supplement, 100 U/mL of penicillin, and 100 μg/mL of streptomycin.

Mouse Studies. Forebrain-specific *Lmnb1* and *Lmnb2* knockout mice (*Emx1-Cre Lmnb1*$^{fl/fl}$, *Emx1-Cre Lmnb2*$^{fl/fl}$) were generated as described (12) and bred with *ROSA*$^{nT\text{-}nG}$ mice (B6;129S4-*Gt(ROSA)26Sor*$^{tm1(CAG\text{-}tdTomato*,\text{-}EGFP*)Ee/s}$/J) from The Jackson Laboratory (Bar Harbor, ME). All mouse studies were carried out in accordance with the recommendations in the *Guide for the Care and Use of Laboratory Animals* of the National Institutes of Health. All mice were fed a chow diet and housed in a virus-free barrier facility with a 12-h light/dark cycle. Animal protocols were reviewed and approved by the Animal Research Committee of UCLA.

Immunohistochemistry. Mouse tissues were prepared for immunohistochemical studies as described (12). Embryonic brains were fixed in 4% paraformaldehyde in PBS for 2 h at room temperature, incubated in 30% sucrose in PBS at 4 °C overnight, and then frozen in O.C.T. (Tissue-Tek, Sakura Finetek). Sections (10 μm thick) were fixed for 5 min in 4% paraformaldehyde or ice-cold methanol, followed by 5 dips in acetone and permeabilization with 0.1% Tween-20. Background staining with mouse antibodies was minimized with the Mouse-on-Mouse Kit (Vector Laboratories, Burlingame, CA). Tissue sections were blocked with 2.5% horse serum for 1 h at room temperature and incubated overnight at 4 °C with primary antibodies at the dilutions indicated in *SI Appendix*, Table S2. Alexa Fluor 488- and Alexa Fluor 568-conjugated secondary antibodies (Molecular Probes, Invitrogen, Carlsbad, CA) were used at a 1:2,000 dilution; DyLight 649-conjugated streptavidin (Vector Laboratories) was used at 5 μg/mL. After counterstaining with DAPI, sections were mounted with Prolong Gold antifade (Invitrogen) and images were obtained with a Zeiss LSM700 laser-scanning microscope with a Plan Apochromat 20×/0.80 objective (air) or a Plan Apochromat 100×/1.40 oil-immersion objective. Images along the *z* axis were processed by Zen 2010 software (Zeiss).

Fluorescent Vital Dye Staining of Embryonic Tissues. Cerebral cortex explants were harvested from E18.5 mouse embryos and placed in PBS containing 1% BSA. Cell viability was assessed by incubating 2-mm-thick pieces of explants with the LIVE/DEAD fluorescent dye (Thermo Fisher) for 15 min at 20 to 25 °C. After fixation with 4% paraformaldehyde in PBS and staining with DAPI, the tissues were immediately imaged with a Zeiss LSM 700 laser-scanning microscope with a Plan Apochromat 20×/0.80 objective (air).

Preparation of Tissues for Electron Microscopy. The cerebral cortex from E18.5 embryos was excised and fixed overnight at 4 °C in a solution containing 4% paraformaldehyde, 2.5% glutaraldehyde, 2.1% sucrose, and 0.1 M sodium cacodylate. On the next day, the samples were rinsed 5 times for 3 min each with 0.1 M sodium cacodylate and then incubated in a solution containing 2% osmium tetroxide, 1.5% potassium ferricyanide, and 0.1 M sodium cacodylate for 1 h at 4 °C. Next, the samples were rinsed 5 times for 3 min each with H_2O and then incubated with 1% thiocarbohydrazide for 20 min at room temperature. Next, samples were rinsed again 5 times for 3 min each with H_2O and then incubated with 2% osmium tetroxide for 30 min at room temperature. The samples were then rinsed 5 times for 3 min with H_2O and incubated with 2% uranyl acetate at 4 °C overnight. On the following day, tissue samples were rinsed with H_2O and dehydrated with a series of increasing ethanol concentrations (30, 50, 70, 85, 95, and 100%) for 10 min each, followed by 2 10-min incubations with 100% ethanol. Next, the samples were infiltrated with Embed812 resin (Electron Microscopy Sciences) by incubating samples in 33% resin (diluted in anhydrous acetone) for 2 h, 66% resin overnight, and 100% resin for 4 h. Samples were then embedded in fresh resin using polypropylene molds (Electron Microscopy Sciences) and polymerized in a vacuum oven at 65 °C for 48 h. After polymerization, samples were removed from the molds; block faces were trimmed, faced, and 65-nm sections were cut using a Leica UC6 μLtramicrotome equipped with a Diatome diamond knife. Sections were collected onto glow-discharged copper grids coated with formvar and carbon (Electron Microscopy Sciences) and stained with Reynold's lead citrate solution for 10 min. Finally, samples were imaged with a FEI Tecnai T12 transmission electron microscope set at 120 kV and equipped with a Gatan CCD camera.

Statistical Analyses. Statistical analyses were performed with GraphPad QuickCalcs (https://www.graphpad.com/). Differences in nuclear morphologies (blebs, irregularly shaped nuclei) and the frequency of NM ruptures were analyzed with a χ^2 test. Differences in nuclear circularity and numbers of γH2AX foci were assessed with a 2-tailed Student's *t* test.

See *SI Appendix, SI Materials and Methods* for more details on the methods we used.

Data Availability. All data are available in the manuscript and *SI Appendix*.

ACKNOWLEDGMENTS. This work was supported by NIH Grants HL126551 (S.G.Y.) and AG047192 (L.G.F.), a NIH Ruth L. Kirschstein National Research Service Award T32GM065823 (N.Y.C.), a Whitcome Fellowship Award from UCLA's Molecular Biology Institute, and a Vascular Biology Training Grant. We acknowledge support provided by NIH/National Center for Advancing Translational Science UCLA Clinical and Translational Science Institute Grant KL2TR001882 as well as Young Investigator Awards from the Alex's Lemonade Stand Foundation for Childhood Cancer Research, Hyundai Hope on Wheels, and the Tower Cancer Research Foundation. We acknowledge Chiara Bertipaglia and Richard Vallee (Columbia University) for helpful discussions. We thank Dr. Janel LeBelle and Dr. Harvey Kornblum (UCLA) for sharing methods for culturing neurospheres. We thank Dr. Jan Lammerding for sharing the NLS-GFP plasmid. We thank Ms. Lisa Kawakami for help with microfabrication and Ms. Liv Heidenreich for help with microstructure functionalization. Virus production and transduction were performed by the Integrated Molecular Technologies Core/UCLA Vector Core, which is supported by CURE/P30 DK041301. Nano- and microfabrication were performed at the Integrated Systems Nanofabrication Cleanroom of the California NanoSystems Institute.

1. J. Harborth, S. M. Elbashir, K. Bechert, T. Tuschl, K. Weber, Identification of essential genes in cultured mammalian cells using small interfering RNAs. *J. Cell Sci.* **114**, 4557–4565 (2001).
2. L. Vergnes, M. Péterfy, M. O. Bergo, S. G. Young, K. Reue, Lamin B1 is required for mouse development and nuclear integrity. *Proc. Natl. Acad. Sci. U.S.A.* **101**, 10428–10433 (2004).
3. R. D. Moir, M. Montag-Lowy, R. D. Goldman, Dynamic properties of nuclear lamins: Lamin B is associated with sites of DNA replication. *J. Cell Biol.* **125**, 1201–1212 (1994).
4. R. I. Lopez-Soler, R. D. Moir, T. P. Spann, R. Stick, R. D. Goldman, A role for nuclear lamins in nuclear envelope assembly. *J. Cell Biol.* **154**, 61–70 (2001).
5. M. Y. Tsai *et al*., A mitotic lamin B matrix induced by RanGTP required for spindle assembly. *Science* **311**, 1887–1893 (2006).
6. T. Dechat *et al*., Nuclear lamins: Major factors in the structural organization and function of the nucleus and chromatin. *Genes Dev.* **22**, 832–853 (2008).
7. C. J. Hutchison, Lamins: Building blocks or regulators of gene expression? *Nat. Rev. Mol. Cell Biol.* **3**, 848–858 (2002).
8. S. H. Yang *et al*., An absence of both lamin B1 and lamin B2 in keratinocytes has no effect on cell proliferation or the development of skin and hair. *Hum. Mol. Genet.* **20**, 3537–3544 (2011).
9. S. H. Yang, H. J. Jung, C. Coffinier, L. G. Fong, S. G. Young, Are B-type lamins essential in all mammalian cells? *Nucleus* **2**, 562–569 (2011).
10. C. Coffinier, L. G. Fong, S. G. Young, LINCing lamin B2 to neuronal migration: Growing evidence for cell-specific roles of B-type lamins. *Nucleus* **1**, 407–411 (2010).
11. C. Coffinier *et al*., Abnormal development of the cerebral cortex and cerebellum in the setting of lamin B2 deficiency. *Proc. Natl. Acad. Sci. U.S.A.* **107**, 5076–5081 (2010).
12. C. Coffinier *et al*., Deficiencies in lamin B1 and lamin B2 cause neurodevelopmental defects and distinct nuclear shape abnormalities in neurons. *Mol. Biol. Cell* **22**, 4683–4693 (2011).
13. S. G. Young, H. J. Jung, C. Coffinier, L. G. Fong, Understanding the roles of nuclear A- and B-type lamins in brain development. *J. Biol. Chem.* **287**, 16103–16110 (2012).
14. T. Shimi *et al*., The A- and B-type nuclear lamin networks: Microdomains involved in chromatin organization and transcription. *Genes Dev.* **22**, 3409–3421 (2008).
15. R. D. Moir *et al*., Review: The dynamics of the nuclear lamins during the cell cycle–relationship between structure and function. *J. Struct. Biol.* **129**, 324–334 (2000).
16. C. W. Tang *et al*., The integrity of a lamin-B1-dependent nucleoskeleton is a fundamental determinant of RNA synthesis in human cells. *J. Cell Sci.* **121**, 1014–1024 (2008).
17. R. B. Vallee, J. W. Tsai, The cellular roles of the lissencephaly gene LIS1, and what they tell us about brain development. *Genes Dev.* **20**, 1384–1393 (2006).
18. J. W. Tsai, K. H. Bremner, R. B. Vallee, Dual subcellular roles for LIS1 and dynein in radial neuronal migration in live brain tissue. *Nat. Neurosci.* **10**, 970–979 (2007).
19. D. J. Hu *et al*., Dynein recruitment to nuclear pores activates apical nuclear migration and mitotic entry in brain progenitor cells. *Cell* **154**, 1300–1313 (2013).
20. A. Gupta, L. H. Tsai, A. Wynshaw-Boris, Life is a journey: A genetic look at neocortical development. *Nat. Rev. Genet.* **3**, 342–355 (2002).
21. A. Wynshaw-Boris, Lissencephaly and LIS1: Insights into the molecular mechanisms of neuronal migration and development. *Clin. Genet.* **72**, 296–304 (2007).
22. H. J. Jung *et al*., Farnesylation of lamin B1 is important for retention of nuclear chromatin during neuronal migration. *Proc. Natl. Acad. Sci. U.S.A.* **110**, E1923–E1932 (2013).
23. J. D. Vargas, E. M. Hatch, D. J. Anderson, M. W. Hetzer, Transient nuclear envelope rupturing during interphase in human cancer cells. *Nucleus* **3**, 88–100 (2012).
24. E. M. Hatch, A. H. Fischer, T. J. Deerinck, M. W. Hetzer, Catastrophic nuclear envelope collapse in cancer cell micronuclei. *Cell* **154**, 47–60 (2013).
25. E. Hatch, M. Hetzer, Breaching the nuclear envelope in development and disease. *J. Cell Biol.* **205**, 133–141 (2014).
26. C. M. Denais *et al*., Nuclear envelope rupture and repair during cancer cell migration. *Science* **352**, 353–358 (2016).
27. N. Y. Chen *et al*., Fibroblasts lacking nuclear lamins do not have nuclear blebs or protrusions but nevertheless have frequent nuclear membrane ruptures. *Proc. Natl. Acad. Sci. U.S.A.* **115**, 10100–10105 (2018).
28. H. J. Jung *et al*., Regulation of prelamin A but not lamin C by miR-9, a brain-specific microRNA. *Proc. Natl. Acad. Sci. U.S.A.* **109**, E423–E431 (2012).
29. H. J. Jung, J. M. Lee, S. H. Yang, S. G. Young, L. G. Fong, Nuclear lamins in the brain - new insights into function and regulation. *Mol. Neurobiol.* **47**, 290–301 (2013).
30. S. G. Young, H. J. Jung, J. M. Lee, L. G. Fong, Nuclear lamins and neurobiology. *Mol. Cell. Biol.* **34**, 2776–2785 (2014).
31. J. M. Lee *et al*., Reciprocal knock-in mice to investigate the functional redundancy of lamin B1 and lamin B2. *Mol. Biol. Cell* **25**, 1666–1675 (2014).
32. B. Nadarajah, P. Alifragis, R. O. Wong, J. G. Parnavelas, Neuronal migration in the developing cerebral cortex: Observations based on real-time imaging. *Cereb. Cortex* **13**, 607–611 (2003).
33. B. S. J. Davies *et al*., Posttranslational processing of nuclear lamins. *Enzymes* **29**, 21–41 (2011).
34. D. Razafsky, N. Blecher, A. Markov, P. J. Stewart-Hutchinson, D. Hodzic, LINC complexes mediate the positioning of cone photoreceptor nuclei in mouse retina. *PLoS One* **7**, e47180 (2012).
35. D. Razafsky *et al*., Lamin B1 and lamin B2 are long-lived proteins with distinct functions in retinal development. *Mol. Biol. Cell* **27**, 1928–1937 (2016).
36. B. H. Toyama *et al*., Identification of long-lived proteins reveals exceptional stability of essential cellular structures. *Cell* **154**, 971–982 (2013).
37. C. M. Gigante *et al*., Lamin B1 is required for mature neuron-specific gene expression during olfactory sensory neuron differentiation. *Nat. Commun.* **8**, 15098 (2017).
38. A. C. Rowat *et al*., Nuclear envelope composition determines the ability of neutrophil-type cells to passage through micron-scale constrictions. *J. Biol. Chem.* **288**, 8610–8618 (2013).